











RESEARCH ARTICLE

Intracranial mesenchymal tumors with FET-CREB fusion are composed of at least two epigenetic subgroups distinct from meningioma and extracranial sarcomas

Emily A. Sloan^{1,2}  | Rohit Gupta¹ | Christian Koelsche³  | Jason Chiang⁴  |
 Javier E. Villanueva-Meyer⁵ | Sanda Alexandrescu⁶  | Jennifer M. Eschbacher⁷ |
 Wesley Wang⁸  | Manuela Mafra⁹ | Nasir Ud Din¹⁰ | Emily Carr-Boyd¹¹ |
 Michael Watson¹¹ | Michael Punsoni¹² | Angelica Oviedo¹³ | Ahmed Gilani¹⁴ |
 Bette K. Kleinschmidt-DeMasters¹⁴ | Dylan J. Coss¹⁵ | M. Beatriz Lopes¹⁵  |
 Alyssa Reddy^{16,17} | Sabine Mueller^{16,17,19} | Soo-Jin Cho¹ | Andrew E. Horvai¹ |
 Julieann C. Lee¹  | Melike Pekmezci¹  | Tarik Tihan¹ | Andrew W. Bollen¹ |
 Fausto J. Rodriguez¹⁸  | David W. Ellison⁴  | Arie Perry^{1,19} | Andreas von Deimling^{20,21} |
 Susan M. Chang¹⁹ | Mitchel S. Berger¹⁹ | David A. Solomon¹ 

¹Department of Pathology, University of California, San Francisco, San Francisco, California, USA

²Department of Pathology and Laboratory Medicine, MedStar Georgetown University Hospital, Washington, D.C., USA

³Institute of Pathology, Heidelberg University Hospital, Heidelberg, Germany

⁴Department of Pathology, St. Jude Children's Research Hospital, Memphis, Tennessee, USA

⁵Department of Radiology and Biomedical Imaging, University of California, San Francisco, San Francisco, California, USA

⁶Department of Pathology, Boston Children's Hospital, Harvard Medical School, Boston, Massachusetts, USA

⁷Department of Neuropathology, Barrow Neurological Institute, St Joseph's Hospital and Medical Center, Phoenix, Arizona, USA

⁸Department of Pathology, The Ohio State University, Columbus, Ohio, USA

⁹Department of Pathology, The Portuguese Institute of Oncology, Lisbon, Portugal

¹⁰Section of Histopathology, Department of Pathology and Laboratory Medicine, Aga Khan University Hospital, Karachi, Pakistan

¹¹Department of Histopathology, ADHB LabPlus, Auckland, New Zealand

¹²Department of Pathology, University of Nebraska Medical Center, Omaha, Nebraska, USA

¹³Department of Anatomic Pathology, Dalhousie University, Halifax, Nova Scotia, Canada

¹⁴Department of Pathology, University of Colorado, Aurora, Colorado, USA

¹⁵Department of Pathology, Neuropathology Division, University of Virginia Health System, Charlottesville, Virginia, USA

¹⁶Department of Pediatrics, University of California, San Francisco, San Francisco, California, USA

¹⁷Department of Neurology, University of California, San Francisco, San Francisco, California, USA

¹⁸Department of Pathology, Johns Hopkins University School of Medicine, Baltimore, Maryland, USA

¹⁹Department of Neurological Surgery, University of California, San Francisco, San Francisco, California, USA

²⁰Department of Neuropathology, Heidelberg University Hospital, Heidelberg, Germany

²¹German Cancer Research Center (DKFZ), German Consortium for Translational Cancer Research (DKTK), Heidelberg, Germany

Emily A. Sloan and Rohit Gupta contributed equally to this study.

This is an open access article under the terms of the [Creative Commons Attribution-NonCommercial-NoDerivs](https://creativecommons.org/licenses/by-nc-nd/4.0/) License, which permits use and distribution in any medium, provided the original work is properly cited, the use is non-commercial and no modifications or adaptations are made.

© 2021 The Authors. *Brain Pathology* published by John Wiley & Sons Ltd on behalf of International Society of Neuropathology.

Correspondence

David A. Solomon, Department of Pathology, University of California, San Francisco, 513 Parnassus Ave, Health Sciences West 451, San Francisco, CA 94143, USA.
Email: david.solomon@ucsf.edu

Funding information

National Cancer Institute, Grant/Award Number: P50 CA097257; NIH Office of the Director, Grant/Award Number: DP5 OD021403

Abstract

‘Intracranial mesenchymal tumor, FET-CREB fusion-positive’ occurs primarily in children and young adults and has previously been termed intracranial angiomatoid fibrous histiocytoma (AFH) or intracranial myxoid mesenchymal tumor (IMMT). Here we performed genome-wide DNA methylation array profiling of 20 primary intracranial mesenchymal tumors with FET-CREB fusion to further study their ontology. These tumors resolved into two distinct epigenetic subgroups that were both divergent from all other analyzed intracranial neoplasms and soft tissue sarcomas, including meningioma, clear cell sarcoma of soft tissue (CCS), and AFH of extracranial soft tissue. The first subgroup (Group A, 16 tumors) clustered nearest to but independent of solitary fibrous tumor and AFH of extracranial soft tissue, whereas the second epigenetic subgroup (Group B, 4 tumors) clustered nearest to but independent of CCS and also lacked expression of melanocytic markers (HMB45, Melan A, or MITF) characteristic of CCS. Group A tumors most often occurred in adolescence or early adulthood, arose throughout the neuroaxis, and contained mostly *EWSR1-ATF1* and *EWSR1-CREB1* fusions. Group B tumors arose most often in early childhood, were located along the cerebral convexities or spinal cord, and demonstrated an enrichment for tumors with *CREM* as the fusion partner (either *EWSR1-CREM* or *FUS-CREM*). Group A tumors more often demonstrated stellate/spindle cell morphology and hemangioma-like vasculature, whereas Group B tumors more often demonstrated round cell or epithelioid/rhabdoid morphology without hemangioma-like vasculature, although robust comparison of these clinical and histologic features requires future study. Patients with Group B tumors had inferior progression-free survival relative to Group A tumors (median 4.5 vs. 49 months, $p = 0.001$). Together, these findings confirm that intracranial AFH-like neoplasms and IMMT represent histologic variants of a single tumor type (‘intracranial mesenchymal tumor, FET-CREB fusion-positive’) that is distinct from meningioma and extracranial sarcomas. Additionally, epigenomic evaluation may provide important prognostic subtyping for this unique tumor entity.

KEY WORDS

angiomatoid fibrous histiocytoma (AFH), *ATF1*, brain tumor, clear cell sarcoma, *CREB1*, *CREM*, *EWSR1*, intracranial mesenchymal tumor with FET-CREB fusion, intracranial myxoid mesenchymal tumor, molecular neuropathology, sarcoma

1 | INTRODUCTION

The newly recognized World Health Organization (WHO) tumor type, ‘intracranial mesenchymal tumor, FET-CREB fusion-positive’ [1], is a rare neoplasm of the central nervous system (CNS) that has been previously described as either intracranial angiomatoid fibrous histiocytoma or intracranial myxoid mesenchymal tumor (IMMT) [2–5]. This tumor is molecularly defined by in-frame gene fusion of the FET family of RNA-binding

proteins (*EWSR1* or *FUS*) to the CREB (cyclic AMP response element binding protein) family of transcription factors, which includes *ATF1*, *CREB1*, and *CREM*. Notably, identical FET-CREB fusions are recurrently found in angiomatoid fibrous histiocytoma (AFH), clear cell sarcoma of soft tissue (CCS), clear cell sarcoma of the gastrointestinal tract, primary pulmonary myxoid sarcoma, hyalinizing clear cell carcinoma of the salivary gland, and a subset of malignant mesotheliomas lacking *BAP1* and *NF2* alterations [6–16]. However, the exact

relationship of these intracranial mesenchymal tumors with FET-CREB fusions to AFH of extracranial soft tissue and other FET-CREB fusion-driven neoplasms has been uncertain.

We previously studied the clinical, radiologic, histologic, and genomic features of a cohort of 20 intracranial mesenchymal tumors with FET-CREB fusions [5]. We identified that these tumors occur with a female predominance (approximately 2:1 female/male ratio) in a wide age range, but most often occur in the second and third decades of life. They are predominantly extra-axial or intraventricular tumors which can arise throughout the neuroaxis, including the falx, tentorium, cerebral convexities, and lateral ventricles. They are typically contrast enhancing masses, well-circumscribed, with solid and cystic growth patterns, and often have pronounced peritumoral edema. Beyond the oncogenic FET-CREB fusions, they typically lack accompanying oncogenic mutations, amplifications, or deletions, and usually harbor near-diploid genomes. These tumors are associated with a propensity for local recurrence over time, but only a small subset have disseminated and resulted in patient mortality.

Here we have performed genome-wide DNA methylation profiling on our previously published cohort of 20 primary intracranial mesenchymal tumors with FET-CREB fusions to further study the ontology of these neoplasms and identify any clinically relevant epigenetic subgroups.

2 | MATERIALS AND METHODS

2.1 | Study population and tumor specimens

The study cohort consisted of 20 patients who underwent surgical resection of a primary intracranial neoplasm that was identified to harbor a gene fusion of *EWSR1* or the related *FUS* together with a CREB family member (*ATF1*, *CREB1*, or *CREM*). The clinical features of these 20 patients and histopathologic features of the tumor cohort were previously reported [5].

2.2 | Genome-wide DNA methylation profiling

Tumor tissue was selectively scraped from unstained slides or punched from formalin-fixed, paraffin-embedded (FFPE) blocks using 2.0 mm disposable biopsy punches (Integra Miltex Instruments) to enrich for the highest tumor content possible. Genomic DNA was extracted from this macrodissected tumor tissue using the QIAamp DNA FFPE Tissue Kit (Qiagen). Genomic DNA was bisulfite converted using the EZ DNA Methylation kit following the manufacturer's recommended protocol (Zymo Research). Bisulfite converted DNA was then amplified, fragmented, and hybridized

to Infinium EPIC 850k Human DNA Methylation BeadChips following the manufacturer's recommended protocol (Illumina).

2.3 | Processing and quality assessment of DNA methylation data

Methylation data were preprocessed using the minfi package (v.1.30.0) in R Bioconductor (version 3.5.3) [17]. The detection p-value for each sample was computed, and CpG sites with detection *p* values above 0.05 were discarded from the analysis. Additional quality control was performed by calculating the median log (base2) intensities for methylated and unmethylated signals for each array. All samples had unmethylated and methylated median intensity values above 10 that were used for analysis. Functional normalization with NOOB background correction and dye-bias normalization was performed [18, 19]. Probe filtering was performed after normalization. Specifically, probes located on sex chromosomes, containing nucleotide polymorphisms (dbSNP132 Common) within five base pairs of and including the targeted CpG site, or mapping to multiple sites on hg19 (allowing for one mismatch), as well as cross reactive probes were removed from analysis.

2.4 | Unsupervised hierarchical clustering of DNA methylation data

We performed unsupervised hierarchical clustering with the *hclust* function in Rstats (v3.6.0) to assess variation in DNA methylation patterns and determine any relevant epigenetic subgrouping among the 20 tumors. The *lmFit* function from the Limma package (v.3.40.6) was applied on a log-transformed β -value matrix to identify the 20,000 most differentially methylated CpG probes across the tumor cohort. Then K-means clustering utilizing the Pearson distance matrix with complete linkage was used to determine the optimal number of clusters, through 500 re-sampling interactions of the dataset for K-means of 2, 3, 4, or 5. Visualization was performed using the R package ComplexHeatmap (v.2.0.0) [20].

We also compared the DNA methylation patterns of the 20 intracranial mesenchymal tumors with FET-CREB fusion against the DNA methylation patterns of two extracranial sarcoma entities with identical FET-CREB fusions (clear cell sarcoma of soft tissue and angiomatoid fibrous histiocytoma) that we recently generated as part of our development of the DKFZ Sarcoma Methylation Classifier (www.molecularsarcomapathology.org) [21]. This included 7 reference cases of clear cell sarcoma of soft parts (tumor ID's: 956, 957, 958, 959, 960, 961, and 962), which were all located in the soft tissue of the upper or lower extremities with median patient age of 56 years (range 18–78 years). Also included

were 8 reference cases of angiomatoid fibrous histiocytoma (tumor ID's: 340, 341, 360, 361, 362, 363, 364, 1066), which were all located in extracranial soft tissue with median patient age of 11 years (range 6–13 years). The `lmFit` function from the `Limma` package (v.3.40.6) was applied on a log-transformed β -value matrix to identify the 20,000 most differentially methylated CpG probes across the cohort of 20 intracranial mesenchymal tumors with FET-CREB fusion together with the 7 reference cases of clear cell sarcoma of soft parts and 8 reference cases of angiomatoid fibrous histiocytoma of extracranial soft tissue. K-means clustering utilizing the Pearson distance matrix with complete linkage was then used to determine the optimal number of clusters, through 500 re-sampling interactions of the dataset for K-means of 2, 3, 4, or 5. Unsupervised hierarchical clustering of DNA methylation data was performed using the `hclust` function in `Rstats` (v3.6.0). Visualization was performed using the `R` package `ComplexHeatmap` (v.2.0.0).

2.5 | tSNE dimensionality reduction of DNA methylation data

The DNA methylation profiles of the 20 intracranial mesenchymal tumors with FET-CREB fusions were assessed together with 210 reference tumors spanning 17 sarcoma and CNS tumor entities previously generated at DKFZ [21, 22], which were selected based on tumor types with a similar meningeal/extra-axial location, tumor types that might enter into the differential diagnosis based on overlapping morphologic appearance, and extracranial sarcomas driven by *EWSR1* or *FUS* gene fusions. These included 10 angiomatoid fibrous histiocytoma of extracranial soft tissue, 30 atypical teratoid/rhabdoid tumor (belonging to the three different epigenetic subgroups: MYC, SHH, and TYR), 10 clear cell sarcoma of soft tissue, 10 chordoma, 10 extraskeletal myxoid chondrosarcoma, 10 H3 K27M-mutant diffuse midline glioma, 10 desmoplastic small round cell tumor, 10 Ewing sarcoma, 10 IDH-wildtype glioblastoma of the mesenchymal epigenetic subclass, 10 low-grade fibromyxoid sarcoma, 30 meningioma (belonging to the various epigenetic subgroups), 10 alveolar rhabdomyosarcoma, 10 embryonal rhabdomyosarcoma, 10 *CIC*-altered sarcoma, 10 *DICER1*-mutant sarcoma, 10 solitary fibrous tumor, and 10 synovial sarcoma. Since the reference cohort contained methylation data generated using the Infinium Human Methylation 450k BeadChips, the approximately 450,000 overlapping CpG sites between the EPIC 850k and 450k BeadChips were used in the analysis. A beta value matrix with approximately 390,000 CpG probes was used for all downstream analysis. Row-wise standard deviation was calculated for each probe across all samples, and the 20,000 most differentially methylated probes with standard deviation >0.216 were selected. Dimensionality reduction using t-distributed

stochastic neighbor embedding (tSNE) was performed by `Rtsne` (v.0.15) using the following analysis parameters: `dims = 2`, `max_iter = 3000`, `theta = 0`, `perplexity = 20`, `eta = 200`. The tSNE plot was visualized with `ggplot2` (v.3.2.0) [<https://ggplot2.tidyverse.org/>].

2.6 | Differentially methylated region and gene ontology analysis

Differentially methylated regions (DMRs) between epigenetic tumor classes were identified using `DMRcate` (v.1.20.0) [23], which ranks the most differentially methylated genomic regions using gaussian smoothing across adjacent CpG sites. For `DMRcate`, a model with coefficients using the following parameters and thresholds was created: `lambda` (genomic window length) = 1000 nucleotides, `C` (scaling factor) = 2, and probe false discovery rate (FDR) cutoff of less than 0.05. Results were ranked by Fisher's multiple comparison statistic and filtered for those DMRs with both FDR and Stouffer scores less than 0.001. DMRs were then annotated to the nearest gene transcriptional start sites, based on ENSEMBL genome annotations. Gene Ontology (GO) analysis of differentially methylated gene regions was performed using the `gometh` function in the `missMethyl` package [24].

2.7 | Immunohistochemistry

Immunohistochemistry was performed on whole formalin-fixed, paraffin-embedded tissue sections using the following antibodies: desmin (Cell Marque, clone D33, undiluted, ER1 antigen retrieval), epithelial membrane antigen (EMA, Leica, clone GP1.4, undiluted, ER1 antigen retrieval), CD99 (Signet, clone CD99, 1:400 dilution, ER1 antigen retrieval), S100 (DAKO, polyclonal, 1:2000 dilution, no antigen retrieval), MUC4 (Millipore, clone 8G7, 1:500 dilution, ER1 antigen retrieval), somatostatin receptor 2A (SSTR2A, Abcam, clone UMB1, 1:2000 dilution, ER2 antigen retrieval), OLIG2 (Immuno Bio Labs, polyclonal, 1:200 dilution, ER1 antigen retrieval), glial fibrillary acidic protein (GFAP, DAKO, polyclonal, 1:3000 dilution, no antigen retrieval), synaptophysin (Cell Marque, polyclonal, 1:100 dilution, ER2 antigen retrieval), CD68 (Leica, clone 514H12, undiluted, ER2 antigen retrieval), cytokeratin AE1/AE3 (Dako, clone AE1/AE3, 1:100 dilution, ER1 antigen retrieval), cytokeratin CAM5.2 (Becton Dickinson, clone CAM5.2, 1:100 dilution, ER1 antigen retrieval), HMB45 (Dako, clone HMB45, undiluted, CC1 antigen retrieval), Melan A (Dako, clone A103, 1:10 dilution, ER1 antigen retrieval), MITF (Dako, clone D5, 1:200 dilution, ER1 antigen retrieval), myogenin (Cell Marque, clone F5D, undiluted, CC1 antigen retrieval), and Ki-67 (Dako, clone Mib1, 1:50 dilution, ER2 antigen retrieval). Immunostaining for desmin, EMA, CD99, S100, MUC4,

SSTR2A, OLIG2, GFAP, synaptophysin, CD68, cytokeratin AE1/AE3, cytokeratin CAM5.2, Melan A, MITF, and Ki-67 was performed in a Leica BOND-III automated stainer. Immunostaining for HMB45 and myogenin was performed in a Ventana BenchMark Ultra automated stainer. Diaminobenzidine was used as the chromogen, followed by hematoxylin counterstain.

2.8 | Kaplan-Meier survival plots and statistical analyses

Clinical outcomes were studied by Kaplan-Meier analysis using GraphPad Prism. The Kaplan-Meier survival analysis was stratified by epigenetic subgroup, and *p* value was calculated by Log-rank (Mantel-Cox) test. Statistical comparison of histologic and immunohistochemical features was performed by Mann-Whitney unpaired two-tailed *t* test using GraphPad Prism.

3 | RESULTS

3.1 | DNA methylation profiling reveals two epigenetic subgroups

We performed genome-wide DNA methylation profiling on our previously published cohort of 20 primary intracranial mesenchymal tumors with FET-CREB fusions. The clinical and radiologic features of these 20 patients and the histopathologic and genomic features of the tumor cohort were previously reported in open access format – <https://onlinelibrary.wiley.com/doi/10.1111/bpa.12918> [5]. Unsupervised hierarchical clustering of the DNA methylation profiles segregated these tumors into two epigenetically distinct subgroups: Group A consisting of 16 tumors and Group B consisting of 4 tumors (Figure 1A and Table 1).

3.2 | Clinical and molecular characteristics of the two epigenetic subgroups

Group A tumors were from 11 females and 5 males with a median age at diagnosis of 15 years (range 12–70 years) (Tables 1 and 2, Figure 1B). The tumors were located throughout the neuroaxis, including the cerebral convexities (*n* = 4), tentorium (*n* = 2), falx (*n* = 2), lateral ventricles (*n* = 4), and cerebellopontine angle (*n* = 4) (Figure 1C). Fusion partners were *EWSRI-ATF1* (*n* = 7), *EWSRI-CREB1* (*n* = 7), and *EWSRI-CREM* (*n* = 2) (Figure 1D). The 4 Group B tumors were exclusively from females with a median age at diagnosis of 7 years (range 4–15 years). The tumors were located along the cerebral convexities (*n* = 3) or spinal cord (*n* = 1). Fusion partners were *EWSRI-ATF1* (*n* = 1), *EWSRI-CREM* (*n* = 2), and *FUS-CREM* (*n* = 1). As previously reported,

these tumors all had near-diploid genomes [5], and we did not observe any recurrent chromosomal copy number changes among either epigenetic subgroup.

3.3 | Differential gene methylation analysis between two epigenetic subgroups

We next determined all differentially methylated genomic regions (DMR) with a mean beta value difference of at least 0.3 between the two epigenetic subgroups, which yielded nearly 1100 such DMR (Tables S1 and S2). Gene Ontology analysis of the most differentially methylated genes between the two epigenetic subgroups revealed networks involved in Rho GTPase signaling (Figure 1E, Table S3), a pathway known to control cell growth, motility, and actin cytoskeletal remodeling.

3.4 | Histologic and immunophenotypic features of the two epigenetic subgroups

We have previously described the wide morphologic spectrum of intracranial mesenchymal tumors with FET-CREB fusion, ranging from stellate/spindle cell to epithelioid/rhabdoid cytology along with variable stromal mucin content and hemangioma-like vasculature [5]. When comparing histologic features between the two epigenetic subgroups, no statistically significant differences were apparent (Figure 2, Table 3). The presence of a myxoid stroma did not strictly correlate with the epigenetic subgroups – 11/16 (69%) of the Group A tumors and 1/4 (25%) of the Group B tumors demonstrated a mucin-rich stroma. Hemangioma-like vasculature was only encountered in the Group A tumors (10/16 [63%]). Stellate/spindle cell cytomorphology was also only encountered in Group A tumors (10/16 [63%]).

The Ki-67 labeling index in this tumor cohort was generally low (less than 5%, 8 of the 15 evaluated tumors), but occasionally was elevated up to 15%–25% (7 of the 15 evaluated tumors) [5]. There was no significant difference in Ki-67 labeling index between the two epigenetic subgroups, though three of the four Group B tumors were those with elevated Ki-67 labeling index.

We also examined for any differences in immunophenotype between the two epigenetic subgroups (Table 4). Desmin, EMA, CD99, and CD68 expression was nearly ubiquitous among all tumors belonging to both subgroups, and MUC4 and synaptophysin expression was also frequent in both subgroups. Among the seven Group A tumors evaluated for MUC4 expression, three demonstrated diffuse strong staining, one demonstrated focal positivity, and two were negative. Among the four Group B tumors evaluated for MUC4 expression, three demonstrated focal positivity and one was negative. Among the seven Group A tumors evaluated for synaptophysin expression, three demonstrated patchy variable

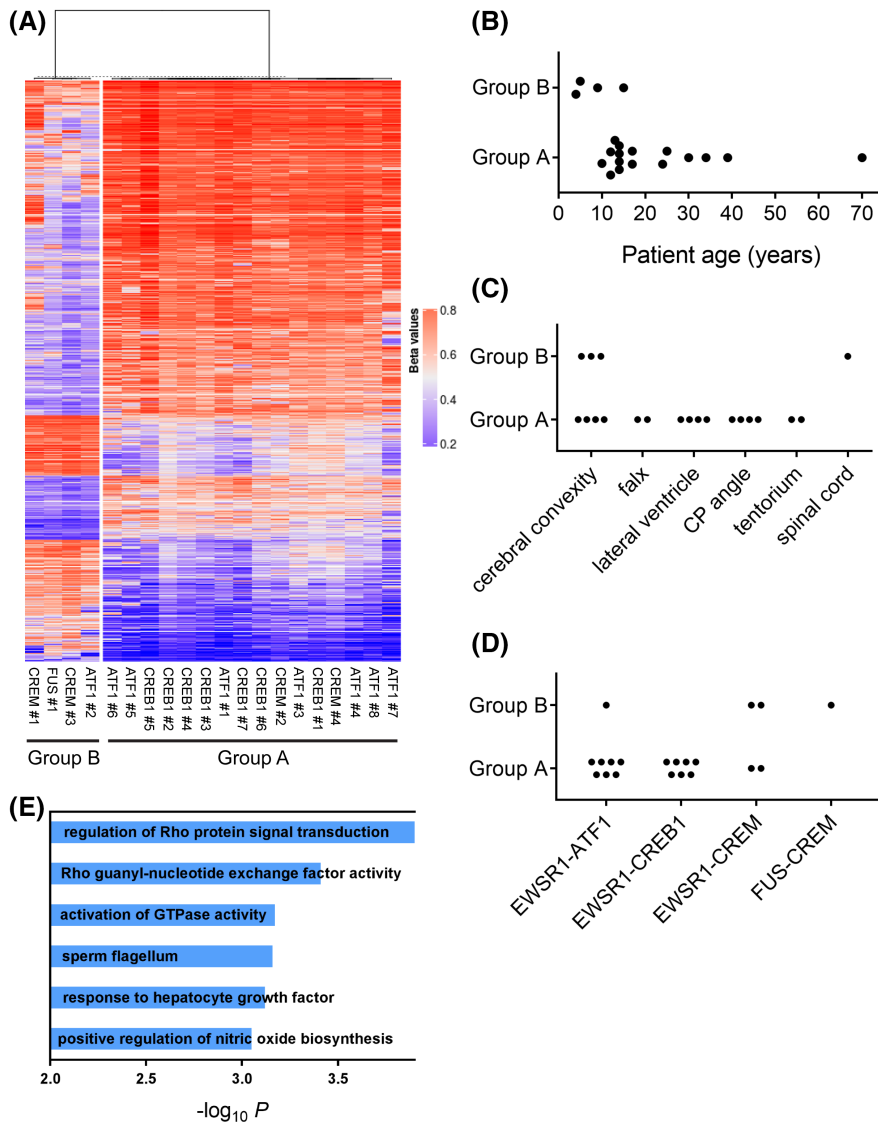


FIGURE 1 ‘Intracranial mesenchymal tumor, FET-CREB fusion-positive’ is composed of two distinct epigenetic subgroups. (A) Unsupervised hierarchical clustering of DNA methylation data from 20 intracranial mesenchymal tumors with FET-CREB fusion showing segregation into two epigenetic subgroups – Group A consisting of 16 tumors and Group B consisting of 4 tumors. Differentially methylated genomic regions between the two subgroups are annotated in Tables S1 and S2. (B) Dot plot of patient age at diagnosis stratified by epigenetic subgroup. (C) Dot plot of tumor anatomic location stratified by epigenetic subgroup. (D) Dot plot of fusion type stratified by epigenetic subgroup. (E) Differential methylation-based gene ontology analysis for the two epigenetic subgroups of intracranial mesenchymal tumors with FET-CREB fusion, represented in a bar plot of $-\log_{10} p$ values for the most differentially methylated gene networks

intensity staining while the other four were negative. Both of the two Group B tumors evaluated for synaptophysin expression demonstrated patchy variable intensity staining. None of the examined tumors belonging to either subgroup was positive for somatostatin receptor 2A (SSTR2A) expression or markers of melanocytic differentiation (MITF, Melan A, and HMB45). None of the investigated proteins had significantly different expression levels between Group A and Group B tumors, and further studies are necessary to identify potential immunohistochemical surrogates for segregating the two epigenetic subgroups.

3.5 | Clinical outcomes of the two epigenetic subgroups

The complete clinical data including extent of resection, treatment regimen, and outcome data from the twenty patients were previously reported [5]. Kaplan-Meier analysis of progression-free survival (PFS) stratified by

epigenetic subgroup revealed inferior outcomes of Group B tumors relative to Group A tumors (median PFS of 4.5 vs. 49 months, $p = 0.001$) (Figure 3). Only three of the 20 patients succumbed to disease during the period of clinical follow-up, all of whom harbored *EWSR1-ATF1* fusions, of which two (ATF1 #6 and ATF1 #7) belonged to Group A and one (ATF1 #2) belonged to Group B. Kaplan-Meier analysis of overall survival stratified by epigenetic subgroup did not reveal a significant difference (data not shown).

3.6 | Epigenetic comparison with other CNS tumor entities and extracranial sarcomas

We next performed tSNE dimensionality reduction of the DNA methylation profiles for the 20 intracranial mesenchymal tumors with FET-CREB fusion together with 210 reference tumors spanning 17 sarcoma and CNS tumor entities previously generated at DKFZ [21, 22] (Table S4). The intracranial mesenchymal tumors with

TABLE 1 Clinical characteristics, tumor histopathologic features, and epigenetic subgroup for the 20 patients with ‘intracranial mesenchymal tumor, FET-CREB fusion-positive’

Patient ID	Age	Sex	Tumor location	Mucin-rich stroma	Predominant morphology	Fusion type	Epigenetic subgroup
ATF1 #1	12	M	Cerebral convexity (parietal)	No	Epithelioid/rhabdoid	EWSR1-ATF1	Group A
ATF1 #3	24	F	Cerebral convexity (occipital)	Yes	Epithelioid/rhabdoid	EWSR1-ATF1	Group A
ATF1 #4	13	F	Cerebral convexity (frontal)	Yes	Stellate/spindled	EWSR1-ATF1	Group A
ATF1 #5	34	F	Tentorium	No	Epithelioid/rhabdoid	EWSR1-ATF1	Group A
ATF1 #6	17	F	CP angle	No	Epithelioid/rhabdoid	EWSR1-ATF1	Group A
ATF1 #7	70	M	CP angle with spinal dissemination	No	Epithelioid/rhabdoid	EWSR1-ATF1	Group A
ATF1 #8	17	F	CP angle	No	Epithelioid/rhabdoid	EWSR1-ATF1	Group A
CREB1 #1	14	F	Lateral ventricle	Yes	Stellate/spindled	EWSR1-CREB1	Group A
CREB1 #2	39	F	Lateral ventricle	Yes	Stellate/spindled	EWSR1-CREB1	Group A
CREB1 #3	10	M	Falx (parietal)	Yes	Stellate/spindled	EWSR1-CREB1	Group A
CREB1 #4	14	F	Lateral ventricle	Yes	Stellate/spindled	EWSR1-CREB1	Group A
CREB1 #5	25	F	CP angle	Yes	Stellate/spindled	EWSR1-CREB1	Group A
CREB1 #6	14	F	Cerebral convexity (parietal)	Yes	Stellate/spindled	EWSR1-CREB1	Group A
CREB1 #7	12	M	Tentorium	Yes	Stellate/spindled	EWSR1-CREB1	Group A
CREM #2	14	F	Lateral ventricle	Yes	Stellate/spindled	EWSR1-CREM	Group A
CREM #4	30	M	Falx (frontal)	Yes	Stellate/spindled	EWSR1-CREM	Group A
ATF1 #2	9	F	Cerebral convexity (frontal)	Yes	Round cell	EWSR1-ATF1	Group B
CREM #1	15	F	Spinal cord (thoracic)	No	Epithelioid/rhabdoid	EWSR1-CREM	Group B
CREM #3	5	F	Cerebral convexity (frontal)	No	Round cell	EWSR1-CREM	Group B
FUS #1	4	F	Cerebral convexity (occipital)	No	Epithelioid/rhabdoid	FUS-CREM	Group B

FET-CREB fusion resolved into two distinct epigenetic subgroups that were both divergent from all other analyzed intracranial neoplasms and soft tissue sarcomas, including meningioma, Ewing sarcoma, extraskeletal myxoid chondrosarcoma, clear cell sarcoma of soft tissue (CCS), and AFH of extracranial soft tissue (Figure 4, top panel). The two epigenetic subgroups identified by unsupervised hierarchical clustering (Figure 1A) were recapitulated by the tSNE dimensionality reduction analysis, with the same 16 tumors aligning with Group A and same 4 tumors aligning with Group B by both analyses (Figure 4, bottom panel). The Group A tumors clustered nearest to but independent of solitary fibrous tumor and AFH of extracranial soft tissue, whereas the Group B tumors clustered nearest to but independent of CCS and the mesenchymal subclass of IDH-wildtype glioblastoma. By random forest classification using both the online DKFZ Sarcoma Classifier tool version 12.2 and the online DKFZ Brain Tumor Classifier tool version 11b4, only 3 of the 16 Group A tumors aligned with the methylation class “Angiomatoid fibrous histiocytoma”

with a calibrated score of greater than 0.9, whereas the remainder of the 13 tumors did not reliably classify as “Angiomatoid fibrous histiocytoma” or any other reference methylation class of sarcoma or CNS tumor (Table S5). None of the 4 Group B tumors reliably classified as “Angiomatoid fibrous histiocytoma”, “Clear cell sarcoma of soft tissue”, or any other reference methylation class of sarcoma or CNS tumor (Table S5).

We next further compared the DNA methylation patterns of the 20 intracranial mesenchymal tumors with FET-CREB fusion against two extracranial sarcoma entities with identical FET-CREB fusions (clear cell sarcoma of soft tissue and angiomatoid fibrous histiocytoma) that were recently generated as part of the DKFZ Sarcoma Methylation Classifier [21]. Unsupervised hierarchical clustering was performed on the 16 Group A tumors together with 8 reference cases of angiomatoid fibrous histiocytoma, which were all located in extracranial soft tissue with a median patient age of 11 years (range 6–13 years). This unsupervised clustering analysis segregated the 24 total tumors into two groups

– one composed of the 16 Group A tumors and the other composed of the 8 AFH of extracranial soft tissue (Figure 5A). We next determined all differentially methylated genomic regions (DMR) with a mean beta value

TABLE 2 Clinical features of the 20 patients with ‘intracranial mesenchymal tumor, FET-CREB fusion-positive’ stratified by epigenetic subgroup

Clinical features	Group A	Group B	All tumors
Age at diagnosis (years)			
Median	15	7	14
Range	12–70	4–15	4–70
Sex			
Male	5	0	5
Female	11	4	15
Tumor location			
Cerebral convexity	4	3	7
Tentorium	2	0	2
Falx	2	0	2
Lateral ventricle	4	0	4
CP angle	4	0	4
Spinal cord	0	1	1
Fusion type			
<i>EWSR1-ATF1</i>	7	1	8
<i>EWSR1-CREB1</i>	7	0	7
<i>EWSR1-CREM</i>	2	2	4
<i>FUS-CREM</i>	0	1	1

difference of at least 0.3 between the Group A intracranial mesenchymal tumors and AFH of extracranial soft tissue, which yielded nearly 600 such DMR (Tables S6 and S7). Gene Ontology analysis of the most differentially methylated gene regions between the Group A tumors and AFH of extracranial soft tissue revealed networks involved in muscle structure development and axial mesoderm formation (Figure 5B, Table S8).

Unsupervised hierarchical clustering was also performed on the 4 Group B tumors together with 7 reference cases of clear cell sarcoma, which were all located in the soft tissue of the upper or lower extremities with median patient age of 56 years (range 18–78 years). This unsupervised clustering analysis segregated the 11 total tumors into two groups – one composed of the 4 Group B tumors and the other composed of the 7 clear cell sarcomas (Figure 6A). The one intracranial mesenchymal tumor with *EWSR1-CREM* fusion (CREM #1) that clustered somewhat nearer to CCS than the other three Group B tumors on tSNE dimensionality reduction segregated together with the Group B tumors and not CCS by this unsupervised hierarchical clustering analysis. We next determined all differentially methylated genomic regions (DMR) with a mean beta value difference of at least 0.3 between the Group B intracranial mesenchymal tumors and CCS of soft tissue, which yielded nearly 700 such DMR (Tables S9 and S10). One of the most differentially methylated genomic regions was the *MITF* gene, which was substantially hypermethylated in the Group B intracranial mesenchymal tumors versus hypomethylated/unmethylated in the CCS tumors (Figure 6B). *MITF* encodes the microphthalmia-associated transcription

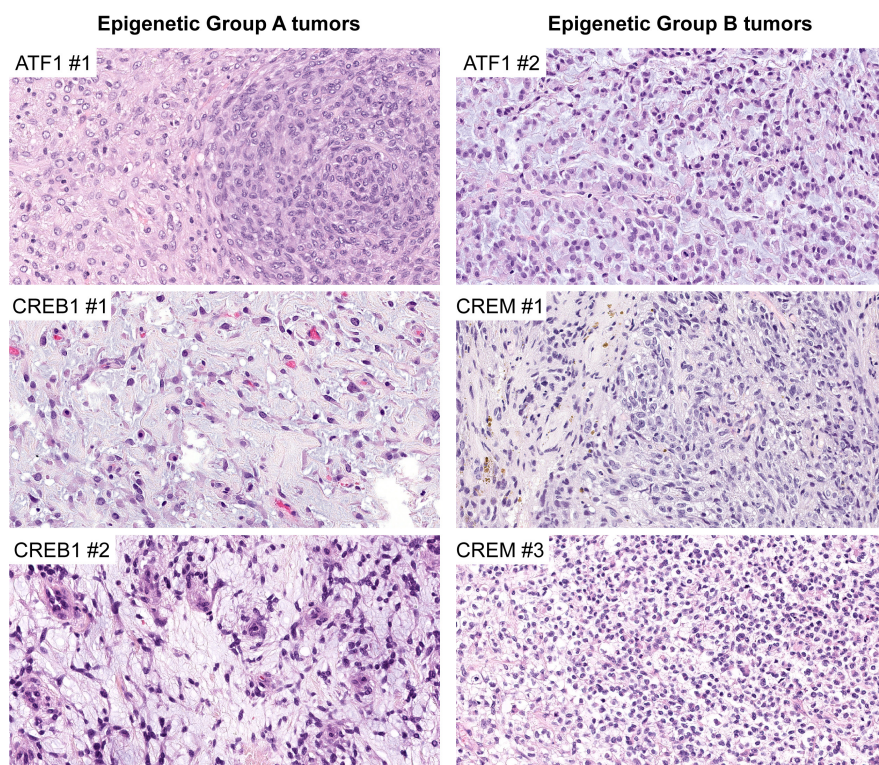


FIGURE 2 Histologic features of intracranial mesenchymal tumors with FET-CREB fusion belonging to the two epigenetic subgroups. Hematoxylin and eosin-stained sections from three representative tumors of the two epigenetic subgroups

TABLE 3 Histologic features of 'intracranial mesenchymal tumor, FET-CREB fusion-positive' stratified by epigenetic subgroup

Histologic feature	Group A	Group B	All tumors
Mucin-rich stroma	11/16 (69%)	1/4 (25%)	12/20 (60%)
Collagenous stroma – intercellular matrix	16/16 (100%)	4/4 (100%)	20/20 (100%)
Collagenous stroma – internodular septae	12/16 (75%)	2/4 (50%)	14/20 (70%)
Epithelioid/rhabdoid morphology	8/16 (50%)	2/4 (50%)	10/20 (50%)
Stellate/spindle cell morphology	10/16 (63%)	0/4 (0%)	10/20 (50%)
Round cell morphology	0/16 (0%)	2/4 (50%)	2/20 (10%)
Hemangioma-like vasculature	10/16 (63%)	0/4 (0%)	10/20 (50%)
Staghorn/HPC-like vasculature	3/16 (19%)	1/4 (25%)	4/20 (20%)
Pseudoangiomatous spaces	0/16 (0%)	0/4 (0%)	0/20 (0%)
Dense lymphoplasmacytic cuffing	11/16 (69%)	1/4 (25%)	12/20 (60%)
Hemosiderin/hematoidin	10/16 (63%)	3/4 (75%)	13/20 (65%)
Meningioma-like whorls	4/16 (25%)	0/4 (0%)	4/20 (20%)
Amianthoid fibers	2/16 (13%)	0/4 (0%)	2/20 (10%)
Necrosis	1/16 (6%)	1/4 (25%)	2/20 (10%)

TABLE 4 Immunohistochemical features of 'intracranial mesenchymal tumor, FET-CREB fusion-positive' stratified by epigenetic subgroup

Protein marker	Group A	Group B	All tumors
Desmin	14/14 (100%)	3/3 (100%)	17/17 (100%)
EMA	13/14 (93%)	3/3 (100%)	16/17 (94%)
CD99	8/8 (100%)	2/2 (100%)	10/10 (100%)
CD68	7/8 (88%)	1/1 (100%)	8/9 (89%)
MUC4	4/7 (57%)	3/4 (75%)	7/11 (64%)
Synaptophysin	3/7 (43%)	2/2 (100%)	5/9 (56%)
S100	6/13 (46%)	1/4 (25%)	7/17 (41%)
SOX10	0/6 (0%)	1/4 (25%)	1/10 (10%)
MelanA	0/2 (0%)	0/4 (0%)	0/6 (0%)
HMB45	0/4 (0%)	0/4 (0%)	0/8 (0%)
MITF	0/1 (0%)	0/4 (0%)	0/5 (0%)
Myogenin	0/6 (0%)	0/2 (0%)	0/8 (0%)
SSTR2a	0/7 (0%)	0/2 (0%)	0/9 (0%)
GFAP	0/10 (0%)	0/2 (0%)	0/12 (0%)
Cytokeratin AE1/AE3	1/10 (10%)	0/1 (0%)	1/11 (9%)
Cytokeratin CAM5.2	0/11 (0%)	0/2 (0%)	0/13 (0%)

factor on chromosome 3p13 that functions as a critical transcription factor for specifying melanocytic differentiation, and is robustly expressed in clear cell sarcoma of soft tissue (formerly referred to as melanoma of soft parts) that is pathologically defined by its expression of melanocytic markers including MITF, HMB45, and Melan A [25, 26]. In contrast to CCS, we found an absence of MITF expression by immunohistochemical staining in all four of the Group B intracranial mesenchymal

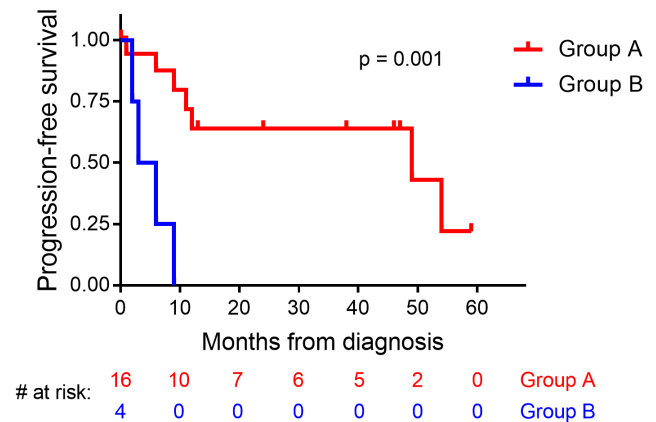


FIGURE 3 Kaplan-Meier plot of progression-free survival for patients with intracranial mesenchymal tumor, FET-CREB fusion-positive stratified by epigenetic subgroup

tumors with FET-CREB fusion, as well as other melanocytic markers (Figure 6C). In addition to MITF, Gene Ontology analysis of the most differentially methylated gene regions between Group B intracranial mesenchymal tumors and CCS of soft tissue revealed networks involved in roof of mouth development and embryonic eye development (Figure 6D, Table S11).

4 | DISCUSSION

Here we have interrogated the epigenomic landscape of intracranial mesenchymal tumors harboring FET-CREB fusion and correlated the results together with clinical and histopathologic features. Our findings reveal that these tumors segregate into two discrete epigenetic

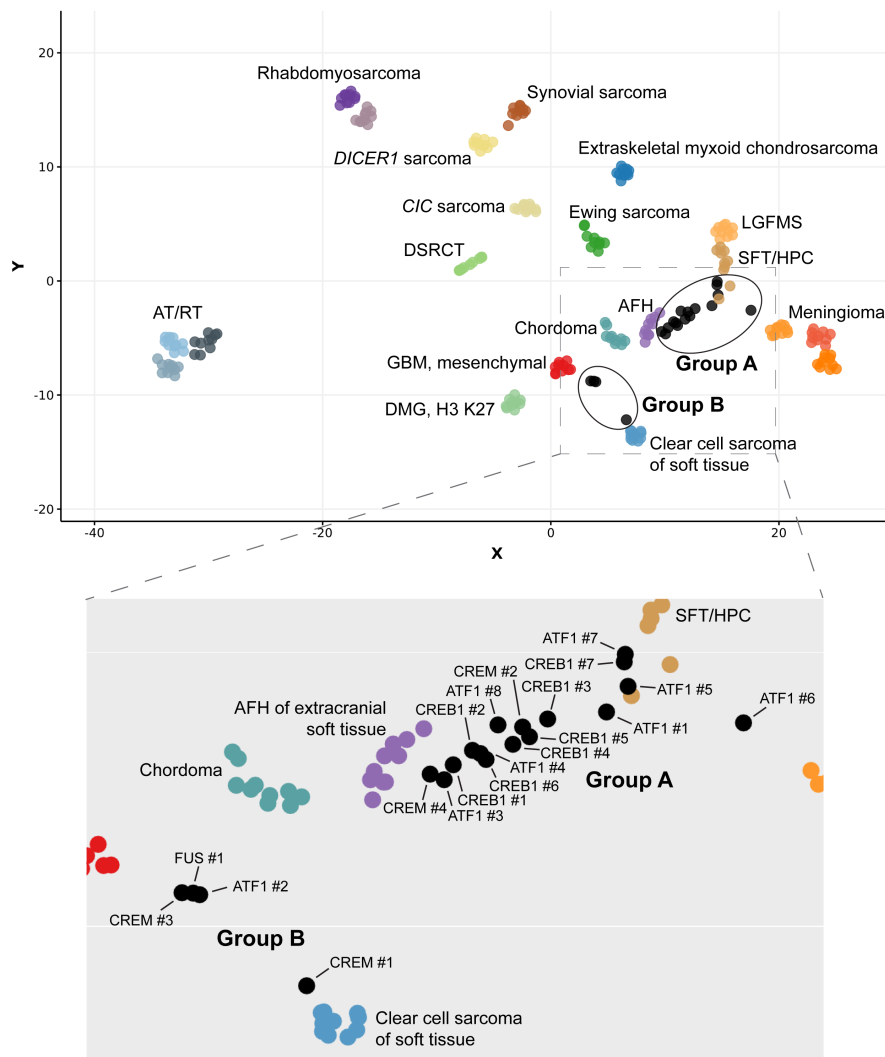


FIGURE 4 tSNE dimensionality reduction plot of genome-wide DNA methylation profiles from the 20 intracranial mesenchymal tumors with FET-CREB fusion alongside 210 reference tumors spanning 17 sarcoma and CNS tumor entities previously generated at DKFZ. See Table S4 for tSNE sample manifest. AT/RT, atypical teratoid/rhabdoid tumor. DMG, diffuse midline glioma. DSRCT, desmoplastic small round cell tumor. GBM, glioblastoma. LGFMS, low-grade fibromyxoid sarcoma. SFT/HPC, solitary fibrous tumor/hemangiopericytoma

subgroups which we have termed Group A and Group B. Group A tumors most often occurred in adolescence or early adulthood, arose throughout the neuroaxis, and consisted of a mix of *EWSRI-ATF1*, *EWSRI-CREB1*, and *EWSRI-CREM* fusions. Group B tumors arose most often in early childhood, were located along the cerebral convexities or spinal cord, and demonstrated an enrichment for tumors with *CREM* as the fusion partner (either *EWSRI-CREM* or *FUS-CREM*). Group A tumors more often demonstrated stellate/spindle cell morphology and hemangioma-like vasculature, whereas Group B tumors more often demonstrated round cell or epithelioid/rhabdoid morphology without hemangioma-like vasculature, although these differences did not reach statistical significance. The presence of a myxoid stroma did not correlate with epigenetic subgrouping, as both epigenetic subgroups contained some tumors with and some without a mucin-rich background. No immunohistochemical differences between the two epigenetic subgroups were identified, and further studies are necessary to test potential immunohistochemical surrogates for segregating the two epigenetic subgroups, perhaps

utilizing the list of most differentially methylated genes as a starting point (Tables S1 and S2). Analysis of patient outcomes demonstrated worse progression-free survival of Group B tumors relative to Group A tumors (median PFS of 4.5 vs. 49 months, respectively), although the cohort size of this study is small and this finding requires further confirmation in larger patient cohorts.

Notably, one of the four tumors that we assigned as belonging to Group B (CREM #1 located in the spinal cord of a 15-year-old female harboring *EWSRI-CREM* fusion) demonstrated a somewhat divergent epigenetic profile relative to the other three tumors within Group B by both unsupervised hierarchical clustering (Figure 1A) and tSNE dimensionality reduction (Figure 4). Despite being in closer proximity to the reference cluster of CCS on the tSNE plot, this tumor CREM #1 more closely grouped with the other Group B tumors than CCS by unsupervised hierarchical clustering (Figure 6A), demonstrated hypermethylation of the *MITF* locus similar to other Group B tumors (Figure 6B), and lacked expression of melanocytic protein markers similar to other Group B tumors (Table 4). Whether this solitary tumor

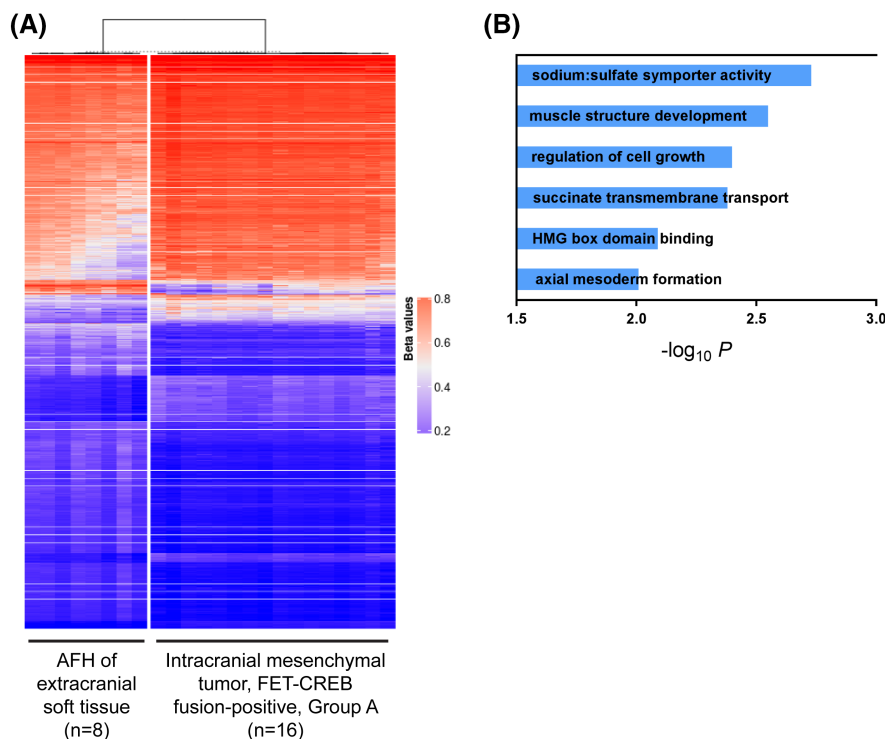


FIGURE 5 Epigenetic comparison of Group A intracranial mesenchymal tumors with FET-CREB fusion to angiomatoid fibrous histiocytoma (AFH) of extracranial soft tissue. (A) Unsupervised hierarchical clustering of DNA methylation data showing segregation of the 16 Group A tumors from 8 reference cases of angiomatoid fibrous histiocytoma arising in extracranial soft tissue. Differentially methylated genomic regions are annotated in Tables S6 and S7. (B) Differential methylation-based gene ontology analysis for Group A intracranial mesenchymal tumors versus AFH of extracranial soft tissue, represented in a bar plot of $-\log_{10} p$ values for the most differentially methylated gene networks

in our cohort is representative of epigenetic heterogeneity amongst Group B tumors or alternatively might represent a third distinct epigenetic subgroup of intracranial mesenchymal tumors with FET-CREB fusion remains uncertain. Future studies with larger patient cohorts are necessary to reveal the full biologic spectrum and clinically relevant subgrouping of these tumors. Overall however, our finding of at least two distinct epigenetic subgroups is similar to a recent report of epigenomic characterization performed on a cohort of 11 primary intracranial mesenchymal tumors with FET-CREB fusion, which identified that 6 of their 11 cases formed a unique epigenetic cluster, whereas the other 5 cases were epigenetically heterogeneous and unclassifiable [27].

For the time being, we believe that these are best considered as two epigenetic subtypes under the single overarching tumor type ‘intracranial mesenchymal tumor, FET-CREB fusion-positive’. This conclusion is based on our cohort of 20 tumors and the fact that there were not statistically significant differences in histomorphology (including stromal mucin content), immunophenotype, fusion partner, patient age, sex, tumor anatomic location, or other features between the two epigenetic subgroups that would enable definitive segregation into two or more distinct tumor types/entities at this point beyond epigenomic signature. However, future studies encompassing larger patient cohorts may potentially indicate

and be used to provide support that these actually represent two or more distinct tumor types.

There has been ongoing uncertainty as to the relationship of tumors diagnosed as “intracranial angiomatoid fibrous histiocytoma” and those diagnosed as “intracranial myxoid mesenchymal tumor”, and we previously proposed the unifying terminology of “intracranial mesenchymal tumor, FET-CREB fusion-positive” for this group of neoplasms [5], which has been adopted in the 5th edition of the WHO Classification of Tumors of the Central Nervous System [1]. There has also been ongoing uncertainty as to the relationship of these intracranial mesenchymal tumors with FET-CREB fusion to meningiomas, as well as to the myriad of extracranial neoplasms harboring identical FET-CREB fusions, which include angiomatoid fibrous histiocytoma, clear cell sarcoma of soft tissue, clear cell sarcoma of the gastrointestinal tract, primary pulmonary myxoid sarcoma, hyalinizing clear cell carcinoma of the salivary gland, and a subset of malignant mesotheliomas lacking *BAP1* and *NF2* alterations [6–16]. Our epigenomic profiling has shed substantial light on these issues that we discuss herein.

First, our epigenomic data, together with the differential immunophenotype (e.g. lack of somatostatin receptor 2A [*SSTR2A*] expression, presence of desmin and *MUC4* expression), further differentiate intracranial

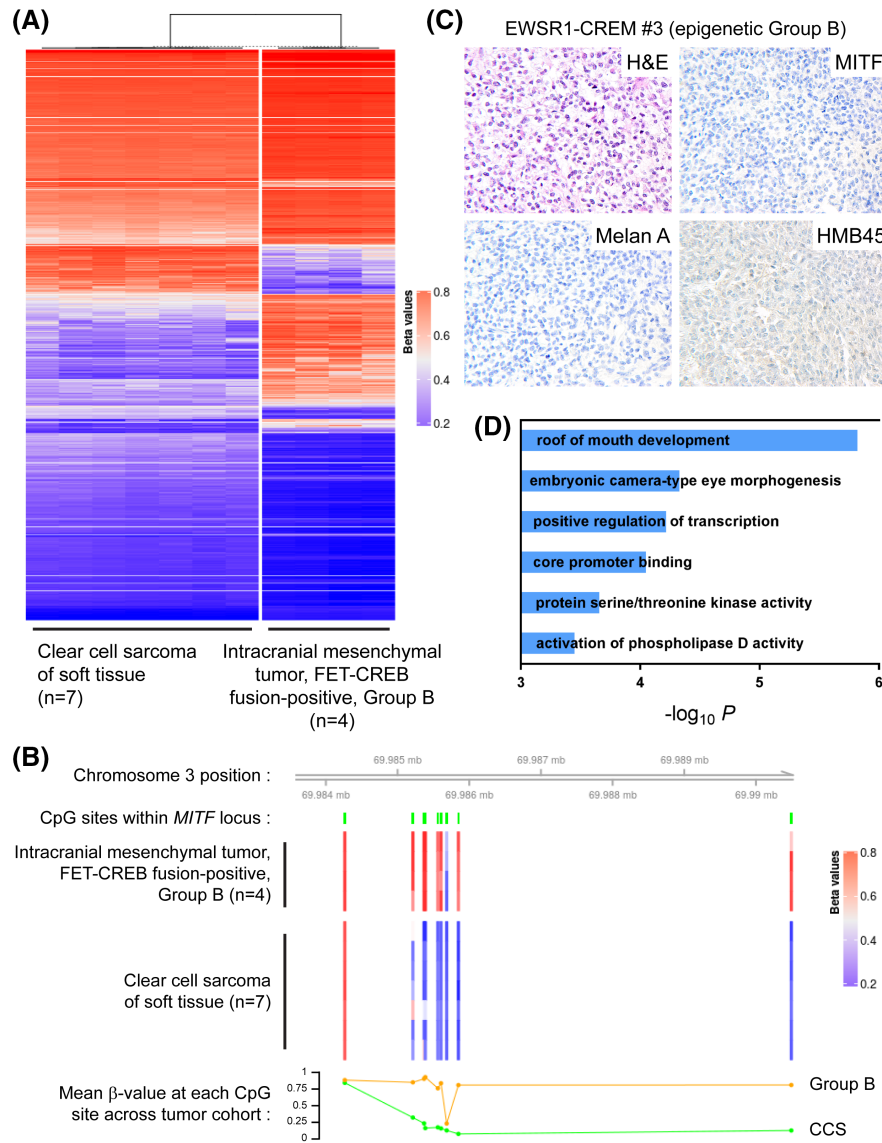


FIGURE 6 Epigenetic comparison of Group B intracranial mesenchymal tumors with FET-CREB fusion to clear cell sarcoma (CCS) of extracranial soft tissue. (A) Unsupervised hierarchical clustering of DNA methylation data showing segregation of the 4 Group B tumors from 7 reference cases of clear cell sarcoma arising in extracranial soft tissue. Differentially methylated genomic regions are annotated in Tables S9 and S10. (B) Visualization of DNA methylation status at individual CpG sites (vertical green bars) at the *MITF* gene locus in the 4 Group B tumors and 7 reference cases of CCS arising in extracranial soft tissue. All but one CpG site demonstrate substantial hypermethylation in the Group B tumors, whereas most all CpG sites are unmethylated or hypomethylated in the CCS tumors. (C) Immunohistochemistry for MITF, a transcription factor robustly expressed in CCS of soft tissue, as well as the other melanocytic markers HMB45 and Melan A, was negative in all four Group B intracranial mesenchymal tumors with FET-CREB fusion. (D) Differential methylation-based gene ontology analysis for Group B intracranial mesenchymal tumors versus CCS of extracranial soft tissue, represented in a bar plot of $-\log_{10} p$ values for the most differentially methylated gene networks

mesenchymal tumors with FET-CREB fusion from meningiomas. However, we cannot exclude a shared cell of origin with meningiomas and/or meningeal solitary fibrous tumors, potentially with epigenetic reprogramming driven by the FET-CREB fusion causing the unique epigenetic signature we found for this tumor type. Further studies are required to define the specific cell of origin of these tumors, which we speculate to be a mesenchymal cell within the meningeal covering of the brain. In support of this hypothesis, electron microscopy performed on intracranial

mesenchymal tumors with FET-CREB fusion has reportedly demonstrated ultrastructural features overlapping with those typically seen in meningioma including interdigitating cell processes lined by well-formed desmosomes and abundant extra-cellular collagen [27].

Second, as both epigenetic subgroups of intracranial mesenchymal tumors with FET-CREB fusion contained some tumors with a mucin-rich stroma resembling “intracranial myxoid mesenchymal tumor” (or the so-called “myxoid variant of AFH”) and also some with a

mucin-poor stroma resembling “intracranial angiomatoid fibrous histiocytoma”, we conclude that these represent histologic variants of a single overarching tumor type. We believe these results further substantiate the unifying nosology of ‘intracranial mesenchymal tumor, FET-CREB fusion-positive’. However, as previously discussed, future studies encompassing larger patient cohorts may potentially indicate and be used to provide support that these epigenetic subgroups among intracranial mesenchymal tumors with FET-CREB fusions actually represent two or more distinct tumor types.

Lastly, we have compared the epigenomic signature of these intracranial mesenchymal tumors with two of the extracranial neoplasms harboring identical FET-CREB fusions for which DNA methylation profiles have been generated to date. Our results reveal that intracranial mesenchymal tumors with FET-CREB fusion are epigenetically distinct from both AFH of extracranial soft tissue and CCS of soft tissue. Given both their distinct epigenetic signature and divergent anatomic site of origin, our results provide further evidence that these tumors should be considered a distinct tumor entity, and not merely regarded as intracranial occurrence of these two sarcomatous neoplasms which characteristically occur in extracranial soft tissue, most often in the extremities. This is particularly true for CCS of soft tissue, given the differential methylation of the *MITF* gene we identified and the absence of melanocytic marker expression in intracranial mesenchymal tumors with FET-CREB fusion.

In summary, we have epigenetically characterized intracranial mesenchymal tumors with FET-CREB fusion, revealing at least two distinct epigenetic subgroups with potential prognostic significance. Our epigenomic results also provide substantial clarification for the ontology of these unique intracranial neoplasms.

ACKNOWLEDGEMENTS

We thank Hong Quach and the staff of the QB3 Functional Genomics Laboratory at the University of California, Berkeley for assistance with DNA methylation array hybridization and scanning. This study was supported by the NIH Director’s Early Independence Award from the Office of the Director, National Institutes of Health (DP5 OD021403) to D.A.S.; a Developmental Research Program Award from the UCSF Brain Tumor SPORE from the National Cancer Institute, National Institutes of Health (P50 CA097257) to D.A.S.; a generous donation from the Morgan Adams Foundation funding kids’ cancer research to D.A.S., a generous donation from the Yuvaan Tiwari Foundation supporting pediatric brain tumor research to D.A.S., and the UCSF Glioblastoma Precision Medicine Program sponsored by the Sandler Foundation.

CONFLICT OF INTEREST

A patent for a DNA methylation-based method for classifying brain tumors has been applied for by DKFZ-Heidelberg University with A.v.D. as an inventor.

B.K.D., F.J.R., D.W.E., A.P., and D.A.S. are on the editorial board of *Brain Pathology*, but were not involved with the assessment or decision-making process for this manuscript. The other authors declare that they have no competing interests.

AUTHOR CONTRIBUTIONS

Emily A. Sloan performed the DNA extractions. Rohit Gupta, Christian Koelsche, Andreas von Deimling, and David A. Solomon performed the epigenomic analysis. Emily A. Sloan and David A. Solomon performed pathologic assessment. Javier E. Villanueva-Meyer performed radiologic assessment. Emily A. Sloan, Jason Chiang, Sanda Alexandrescu, Jennifer M. Eschbacher, Wesley Wang, Manuela Mafra, Nasir Ud Din, Emily Carr-Boyd, Michael Watson, Michael Punsoni, Angelica Oviedo, Ahmed Gilani, Bette K. Kleinschmidt-DeMasters, Dylan J. Coss, M. Beatriz Lopes, Alyssa Reddy, Soo-Jin Cho, Andrew E. Horvai, Julieann C. Lee, Melike Pekmezci, Tarik Tihan, Andrew W. Bollen, Fausto J. Rodriguez, David W. Ellison, Arie Perry, Susan M. Chang, Mitchel S. Berger, and David A. Solomon provided clinical care and contributed to the patient cohort. Emily A. Sloan and David A. Solomon conceptualized the study, reviewed all data, prepared the figures, and wrote the manuscript. Susan M. Chang, Mitchel S. Berger, and David A. Solomon secured funding to support this research study. All authors critically reviewed the manuscript and approved its submission.








ETHICS APPROVAL AND CONSENT TO PARTICIPATE

This study was approved by the Committee on Human Research of the University of California, San Francisco, with a waiver of patient consent.

DATA AVAILABILITY STATEMENT

DNA methylation array data files for the 20 intracranial mesenchymal tumors with FET-CREB fusion generated as part of this study are available from the Gene Expression Omnibus (GEO) repository under accession number [GSE164994 \(https://www.ncbi.nlm.nih.gov/geo/\)](https://www.ncbi.nlm.nih.gov/geo/). Scanned image files of H&E stained sections from 19 of the tumors in this cohort are available for downloading and viewing at the following link: https://figshare.com/projects/Intracranial_mesenchymal_tumors_with_EWS-CREB_fusion/88661.

ORCID

Emily A. Sloan  <https://orcid.org/0000-0002-7268-2712>
Christian Koelsche  <https://orcid.org/0000-0001-8763-8864>
Jason Chiang  <https://orcid.org/0000-0003-3623-8996>
Sanda Alexandrescu  <https://orcid.org/0000-0001-9246-4184>
Wesley Wang  <https://orcid.org/0000-0001-7904-9015>
M. Beatriz Lopes  <https://orcid.org/0000-0001-8661-6727>
Julieann C. Lee  <https://orcid.org/0000-0003-0138-4862>

Melike Pekmezci  <https://orcid.org/0000-0003-2548-8359>
 Fausto J. Rodriguez  <https://orcid.org/0000-0001-8662-1219>
 David W. Ellison  <https://orcid.org/0000-0003-1239-7757>
 David A. Solomon  <https://orcid.org/0000-0003-4571-7999>

REFERENCES

- Louis DN, Perry A, Wesseling P, Brat DJ, Cree IA, Figarella-Branger D, et al. The 2021 WHO Classification of Tumors of the Central Nervous System: a summary. *Neuro-Oncology*. 2021;23(8):1231–1251. <https://doi.org/10.1093/neuonc/noab106>
- Dunham C, Hussong J, Seiff M, Pfeifer J, Perry A. Primary intracerebral angiomatoid fibrous histiocytoma: report of a case with a t(12;22)(q13;q12) causing type 1 fusion of the EWS and ATF-1 genes. *Am J Surg Pathol*. 2008;32:478–84.
- Kao YC, Sung YS, Zhang L, Chen CL, Vaiyapuri S, Rosenblum MK, et al. EWSR1 fusions with CREB family transcription factors define a novel myxoid mesenchymal tumor with predilection for intracranial location. *Am J Surg Pathol*. 2017;41:482–90.
- Bale TA, Oviedo A, Kozakewich H, Giannini C, Davineni PK, Ligon K, et al. Intracranial myxoid mesenchymal tumors with EWSR1-CREB family gene fusions: myxoid variant of angiomatoid fibrous histiocytoma or novel entity? *Brain Pathol*. 2018;28:183–91.
- Sloan EA, Chiang J, Villanueva-Meyer JE, Alexandrescu S, Eschbacher JM, Wang W, et al. Intracranial mesenchymal tumor with FET-CREB fusion—a unifying diagnosis for the spectrum of intracranial myxoid mesenchymal tumors and angiomatoid fibrous histiocytoma-like neoplasms. *Brain Pathol*. 2021;31:e12918.
- Waters BL, Panagopoulos I, Allen EF. Genetic characterization of angiomatoid fibrous histiocytoma identifies fusion of the FUS and ATF-1 genes induced by a chromosomal translocation involving bands 12q13 and 16p11. *Cancer Genet Cytogenet*. 2000;121:109–16.
- Antonescu CR, Tschernyavsky SJ, Woodruff JM, Jungbluth AA, Brennan MF, Ladanyi M. Molecular diagnosis of clear cell sarcoma: detection of EWS-ATF1 and MITF-M transcripts and histopathological and ultrastructural analysis of 12 cases. *J Mol Diagn*. 2002;4:44–52.
- Ferrari A, Casanova M, Bisogno G, Mattke A, Meazza C, Gandola L, et al. Clear cell sarcoma of tendons and aponeuroses in pediatric patients: a report from the Italian and German Soft Tissue Sarcoma Cooperative Group. *Cancer*. 2002;94:3269–76.
- Antonescu CR, Nafa K, Segal NH, Dal Cin P, Ladanyi M. EWS-CREB1: a recurrent variant fusion in clear cell sarcoma—association with gastrointestinal location and absence of melanocytic differentiation. *Clin Cancer Res*. 2006;12:5356–62.
- Antonescu CR, Dal Cin P, Nafa K, Teot LA, Surti U, Fletcher CD, et al. EWSR1-CREB1 is the predominant gene fusion in angiomatoid fibrous histiocytoma. *Genes Chromosomes Cancer*. 2007;46:1051–60.
- Thway K, Nicholson AG, Lawson K, Gonzalez D, Rice A, Balzer B, et al. Primary pulmonary myxoid sarcoma with EWSR1-CREB1 fusion: a new tumor entity. *Am J Surg Pathol*. 2011;35:1722–32.
- Antonescu CR, Katabi N, Zhang L, Sung YS, Seethala RR, Jordan RC, et al. EWSR1-ATF1 fusion is a novel and consistent finding in hyalinizing clear-cell carcinoma of salivary gland. *Genes Chromosomes Cancer*. 2011;50:559–70.
- Skálová A, Weinreb I, Hyrcza M, Simpson RH, Laco J, Agaimy A, et al. Clear cell myoepithelial carcinoma of salivary glands showing EWSR1 rearrangement: molecular analysis of 94 salivary gland carcinomas with prominent clear cell component. *Am J Surg Pathol*. 2015;39:338–48.
- Yoshida A, Wakai S, Ryo E, Miyata K, Miyazawa M, Yoshida KI, et al. Expanding the phenotypic spectrum of mesenchymal tumors harboring the EWSR1-CREB fusion. *Am J Surg Pathol*. 2019;43:1622–30.
- Desmeules P, Joubert P, Zhang L, Al-Ahmadie HA, Fletcher CD, Vakiani E, et al. A subset of malignant mesotheliomas in young adults are associated with recurrent EWSR1/FUS-ATF1 fusions. *Am J Surg Pathol*. 2017;41:980–8.
- Argani P, Harvey I, Nielsen GP, Takano A, Suurmeijer AJH, Voltaggio L, et al. EWSR1/FUS-CREB fusions define a distinctive malignant epithelioid neoplasm with predilection for mesothelial-lined cavities. *Mod Pathol*. 2020;33:2233–43.
- Aryee MJ, Jaffe AE, Corrada-Bravo H, Ladd-Acosta C, Feinberg AP, Hansen KD, et al. Minfi: a flexible and comprehensive Bioconductor package for the analysis of Infinium DNA methylation microarrays. *Bioinformatics*. 2014;30:1363–9.
- Fortin JP, Labbe A, Lemire M, Zanke BW, Hudson TJ, Fertig EJ, et al. Functional normalization of 450k methylation array data improves replication in large cancer studies. *Genome Biol*. 2014;15:503.
- Triche TJ, Weisenberger DJ, Van Den Berg D, Laird PW, Siegmund KD. Low-level processing of Illumina Infinium DNA Methylation BeadArrays. *Nucleic Acids Res*. 2013;41:e90.
- Gu Z, Eils R, Schlesner M. Complex heatmaps reveal patterns and correlations in multidimensional genomic data. *Bioinformatics*. 2016;32:2847–9.
- Koelsche C, Schrimpf D, Stichel D, Sill M, Sahm F, Reuss DE, et al. Sarcoma classification by DNA methylation profiling. *Nat Commun*. 2021;12:498.
- Capper D, Jones DTW, Sill M, Hovestadt V, Schrimpf D, Sturm D, et al. DNA methylation-based classification of central nervous system tumours. *Nature*. 2018;555:469–74.
- Peters TJ, Buckley MJ, Statham AL, Pidsley R, Samaras K, Lord R, et al. De novo identification of differentially methylated regions in the human genome. *Epigenetics Chromatin*. 2015;8:6.
- Phipson B, Maksimovic J, Oshlack A. missMethyl: an R package for analyzing data from Illumina's HumanMethylation450 platform. *Bioinformatics*. 2016;32:286–8.
- Thway K, Fisher C. Tumors with EWSR1-CREB1 and EWSR1-ATF1 fusions: the current status. *Am J Surg Pathol*. 2012;36:e1–e11.
- Thway K, Fisher C. Angiomatoid fibrous histiocytoma: the current status of pathology and genetics. *Arch Pathol Lab Med*. 2015;139:674–82.
- Tauziède-Espariat A, Sievers P, Larousserie F, Benzakoun J, Guillemot D, Pierron G, et al. An integrative histopathological and epigenetic characterization of primary intracranial mesenchymal tumors, FET:CREB-fused broadening the spectrum of tumor entities in comparison with their soft tissue counterparts. *Brain Pathol*. 2021 Jul 27:e13010. <https://doi.org/10.1111/bpa.13010>

SUPPORTING INFORMATION

Additional supporting information may be found in the online version of the article at the publisher's website.

Table S1–S11

TABLE S1 Differentially methylated regions ranked by mean beta-value fold change for those regions which are hypermethylated in Group A tumors relative to Group B tumors

TABLE S2 Differentially methylated regions ranked by mean beta-value fold change for those regions which are hypermethylated in Group B tumors relative to Group A tumors

TABLE S3 Gene Ontology analysis ranked by differentially methylated genes in epigenetic subgroup A versus B of intracranial mesenchymal tumors with FET-CREB fusion



TABLE S4 Sarcoma and CNS tumor reference samples used for tSNE dimensionality reduction in Figure 4

TABLE S5 Clinical features of the 20 patients with 'intracranial mesenchymal tumor, FET-CREB fusion-positive', DNA methylation array data identifiers, epigenetic subgroup, and calibrated scores from random forest classification using the online DKFZ Sarcoma Classifier v12.2

TABLE S6 Differentially methylated regions ranked by mean beta-value fold change for those regions which are hypermethylated in AFH of extracranial soft tissue versus Group A intracranial mesenchymal tumors with FET-CREB fusion

TABLE S7 Differentially methylated regions ranked by mean beta-value fold change for those regions which are hypomethylated in AFH of extracranial soft tissue versus Group A intracranial mesenchymal tumors with FET-CREB fusion

TABLE S8 Gene Ontology analysis ranked by differentially methylated genes in angiomatoid fibrous histiocytoma (AFH) of extracranial soft tissue versus epigenetic Group A of intracranial mesenchymal tumors with FET-CREB fusion

TABLE S9 Differentially methylated regions ranked

by mean beta-value fold change for those regions which are hypermethylated in clear cell sarcoma of soft tissue (CCS) versus Group B intracranial mesenchymal tumors with FET-CREB fusion

TABLE S10 Differentially methylated regions ranked by mean beta-value fold change for those regions which are hypomethylated in clear cell sarcoma of soft tissue (CCS) versus Group B intracranial mesenchymal tumors with FET-CREB fusion

TABLE S11 Gene Ontology analysis ranked by differentially methylated genes in clear cell sarcoma of soft tissue (CCS) versus epigenetic Group B of intracranial mesenchymal tumors with FET-CREB fusion

How to cite this article: Sloan EA, Gupta R, Koelsche C, Chiang J, Villanueva-Meyer JE, Alexandrescu S, et al. Intracranial mesenchymal tumors with FET-CREB fusion are composed of at least two epigenetic subgroups distinct from meningioma and extracranial sarcomas. *Brain Pathol.* 2022;32:e13037. <https://doi.org/10.1111/bpa.13037>